Two-site exchange revisited: a new method for extracting exchange parameters in biological systems

R. V. Mulkern, A. R. Bleier, I. K. Adzamli, R. G. S. Spencer, T. Sandor, and F. A. Jolesz
Department of Radiology, Brigham and Women's Hospital, Harvard Medical School, Boston, Massachusetts 02115

ABSTRACT A new analysis is presented which links real volume fractions, relaxation rates, and intracompartmental exchange rates directly with apparent volume fractions and relaxation rates obtained from biexponential fits of transverse magnetization decay curves. The analysis differs from previous methods in that measurements from two paramagnetic doping levels are used to close the two-site exchange equations. Both the new method and one previously described by Herbst and Goldstein (HG) have been applied to paramagnetically doped whole-blood data sets. Significant differences in the calculated exchange parameters are found between the two methods. A small dependence of the intracellular relaxation rate on extracellular paramagnetic agent concentration, assumed nonexistent with the HG method, is inferred from the new analysis. The analysis was also applied to published data on perfused rat hearts, and we obtained a limited assessment of two-site exchange in this system.

INTRODUCTION

The distribution of tissue water among more or less defined biological compartments, e.g., intracellular, extracellular, etc., or physical compartments, e.g., "free" or macromolecular "bound" water, is a difficult problem to approach quantitatively . Nuclear magnetic resonance (NMR) techniques that measure proton magnetic relaxation rates can, in principle, perform this task. A widely used model for the interpretation of NMR relaxation rate measurements in tissue, or other systems in which water is expected to be distributed among different sites, is that of two-site exchange (1–4). It may be used in conjunction with transverse or longitudinal magnetization decay curves to determine such physical parameters as proton residence times in compartments, volume fractions of compartments, and the intrinsic magnetic relaxation rates in the compartments. The mathematical formulae of the two-site exchange model can be derived from the Bloch equations and a formalism suitable for practical application has been developed by Woessner and McConnel (1, 2). The resulting system of equations for the two-site exchange parameters is, however, underdetermined. Several previous attempts to circumvent this difficulty have either employed mathematical approximations of the complete two-site exchange equations in some appropriate limit, or independent estimates or measurements, of one of the two-site exchange parameters to close the equations (5–15). This permits the extraction of the remaining exchange parameters from a biexponential decomposition of the decay curves. A useful system of equations suitable for extracting exchange parameters in paramagnetically doped blood has been developed by Herbst and Goldstein (13). In their method, an independent measurement of the intracellular transverse relaxation rate in packed red blood cells is used to close the two-site exchange equations. This system represents a somewhat special case since the tissue is easily separated into intra- and extracellular components.

For inseparable biological systems, an alternative method for extracting exchange parameters from NMR relaxation rate measurements has been proposed by Sobol and co-workers (16, 17). In modeling magnetic relaxation data in healthy mouse tissue, these investigators suggested that four proton pools contributed to the observed decay curves. The two most slowly relaxing components were attributed to bound and bulk water and the two quickly decaying "solid-like" components to lipid and protein protons. In their analysis, the assumption was made that the bound water and the solid-like fractions were equal. In addition, assumptions were required concerning fast mixing, via cross-relaxation (18) as opposed to bodily spin transport, between the solid proton pools and the bound water fraction. This allowed the use of a modified two-site exchange model to extract exchange parameters from multicomponent fits to spin–spin, spin–lattice, and rotating frame spin–lattice relaxation decay curves. An increase in the overall data base was made by employing combinations of hard and soft RF pulses to create varying initial conditions for the magnetization in the four proton pools, as originally suggested by Edzes and Samulski (18). Ultimately, however, curve-fitting procedures had to be employed, because the final system of equations was still underdetermined.

0006-3495/02/89/221/12 $2.00

We propose a simplified method for extracting two-site exchange parameters from biexponential fits of transverse magnetization decay curves. The technique relies on closing the two-site exchange equations by performing repeated measurements on a system in which the intrinsic relaxation rates have been modified to two or more levels with the addition of paramagnetic doping agents. It is shown that six experimental parameters are linked directly to the six exchange parameters that characterize the system at both doping levels. As such, no curve fitting is required beyond that used to obtain biexponential decay parameters of the experimental data. We assume that the volume fractions and exchange rates between compartments are the same at both doping levels and that chemical shift effects are negligible. The method places a severe strain on both the applicability of the two-site exchange model and on the reliability of the experimental input data. Therefore, the ability of the method to produce physically acceptable exchange parameters is a test of both.

We have applied the analysis to both separable systems and inseparable systems. For the separable systems we chose paramagnetically doped whole blood since this permits a comparison with previous analyses (11–14), based on the separability of the system. The perfused rat heart data of Mauss et al. (19) permitted us to test the analysis on a system in which exchange between intra-and extracellular spaces has been proposed as the basis for the observed, biexponential relaxation of the transverse magnetization.

METHOD OF EXCHANGE ANALYSIS

The simplest model of two-site exchange is one in which the nuclei under observation jump between two different environments within which the spin–spin relaxation rates need not be the same, though the Larmor frequencies are the same. The model is characterized by six parameters. These are (1) the fractions of the total observed (exchanging) nuclei in each compartment, f and g; (2) the intrinsic spin–spin relaxation rates in each compartment, R_{2f} and R_{2g} (these are the relaxation rates in each compartment in the absence of exchange); at a different doping level of paramagnetic agent, these become $R_{2f'}$ and $R_{2g'}$; (3) the exchange rates between compartments, k_{fg} and k_{gf}, whose reciprocals represent the average residence time of the observed nucleus in volume fractions f and g, respectively.

These parameters are not independent. The volume fractions are normalized once one assumes that only exchanging nuclei are observed so that

$$f + g = 1. \tag{1}$$

In addition, at equilibrium, steady-state conditions are imposed leading to the "detailed balance" condition

$$fk_{fg} - gk_{gf} = 0. \tag{2}$$

These two relations reduce the number of independent two-site exchange parameters to four.

The solution of the Bloch equations for the transverse magnetization in the presence of two-site exchange predicts that the magnetization decays as a normalized biexponential function (1–3). The relaxation rates and the volume fractions associated with this biexponential function do not directly represent the intrinsic relaxation rates and volume fractions in each compartment. Only in the absence of exchange ($k_{fg} = k_{gf} = 0$) are the apparent fractions and relaxation rates simply and directly related to the real volume fractions and relaxation rates in each compartment. In the more general case, nonlinear equations describe the relation between the real parameters and the apparent parameters as measured by the decay of the transverse magnetization. These relations are presented in the Appendix [(A1)–(A6)] where they provide a starting point for the expressions presented below.

Our approach is to assume that paramagnetic doping does not significantly influence the real volume fractions g and f, or the exchange rates k_{fg} and k_{gf}, but only the intrinsic relaxation rates. Under these conditions, a two-site exchange analysis of two biexponential fits at two doping levels results in a system of six equations and six unknowns. These may be inverted to yield the real volume fractions, exchange rates, and intrinsic relaxation rates at both doping levels, as demonstrated in the Appendix.

The experimental decay curves at two different paramagnetic agent concentrations are fit to normalized biexponentials

$$M_1(t)/M_0 = a \exp(-R_{2a}t) + (1 - a) \exp(-R_{2b}t) \tag{3}$$

$$M_2(t)/M_0 = d \exp(-R_{2a'}t) + (1 - d) \exp(-R_{2b'}t). \tag{4}$$

These yield the six experimental quantities a, R_{2a}, R_{2b}, $R_{2a'}$, $R_{2b'}$, and d. M_0 is the net magnetization at time 0. The relaxation rates R_{2a} and $R_{2a'}$ are now chosen, by convention, to be the largest of the two relaxation rates in Eqs. (3) and (4), respectively. The following combinations of these six quantities are defined:

$$B = (R_{2a} + R_{2b})/2 \tag{5}$$

$$C = (R_{2a} - R_{2b})/2 \tag{6}$$

$$E = (R_{2a'} + R_{2b'})/2 \tag{7}$$

$$F = (R_{2a'} - R_{2b'})/2 \tag{8}$$

$$\alpha = 2C(1 - 2a) \tag{9}$$

$$\beta = 2F(1 - 2d) \tag{10}$$

$$\delta = \alpha - \beta \tag{11}$$

$$\Gamma_{\pm} = (4C^2 - \alpha^2)^{1/2} \pm (4F^2 - \beta^2)^{1/2}. \tag{12}$$

From each set of biexponential parameters, the exchange rate k_{gf}, may be solved for in terms of the volume fraction g and the measured biexponential parameters:

$$k_{gf} = \alpha(1 - g) \pm \{[g(1 - g)(2g - 1)^2(4C^2 - \alpha^2)]^{1/2}\}/2g. \tag{13}$$

$$k_{gf} = \beta(1 - g) \pm \{[g(1 - g)(2g - 1)^2(4F^2 - \beta^2)]^{1/2}\}/2g. \tag{14}$$

Equating these two relations allows us to solve for g in terms of the six measured parameters in Eqs. (3) and (4). The ± signs in Eqs. (13) and (14) are a consequence of the nonlinearity of the original system of equations and indicate that there are four ways to equate the two relations. There are, then, four sets of mathematical solutions. These are labeled (+, +), (−, −), (+, −) and (−, +) where the first sign of each pair represents the sign chosen in Eq. (13) and the second sign represents the sign chosen in Eq. (14). In the case of doped blood, only the (+, +) solution was found to yield physically acceptable exchange parameters, i.e., real and positive. Choosing the + sign in both Eqs. (13) and (14), equating the two relations and solving for g, we find:

$$g = [1 \pm \delta/(\Gamma_-^2 + \delta^2)^{1/2}]/2 \tag{15}$$

The choice of the sign in Eq. (15) is arbitrary since changing it merely reverses the roles of f and g as being the big or small volume fractions, respectively. The other possible solutions are discussed in the Appendix where it is shown that the antisymmetric solutions (+, −) and (−, +), will be physically unacceptable in most situations. The exchange rate k_{gf} is given by Eq. (13) or (14) (+ sign in both) and the remaining two-site exchange parameters are given by

$$f = 1 - g \tag{16}$$

$$k_{fg} = gk_{gf}/f \tag{17}$$

$$R_{2f} = \{2B - k_{fg} - k_{gf} + (\alpha - k_{fg} - k_{gf})/(g - f)\}/2 \tag{18}$$

$$R_{2g} = \{2B - k_{fg} - k_{gf} - (\alpha - k_{fg} - k_{gf})/(g - f)\}/2 \tag{19}$$

$$R_{2f'} = \{2E - k_{fg} - k_{gf} + (\beta - k_{fg} - k_{gf})/(g - f)\}/2 \tag{20}$$

$$R_{2g'} = \{2E - k_{fg} - k_{gf} - (\beta - k_{fg} - k_{gf})/(g - f)\}/2 \tag{21}$$

Because of its independence from measurements made on separated compartments, we refer to this analysis as the closed-loop (CL) analysis.

MATERIALS AND METHODS

American Chemical Society (ACS) reagent grade manganese (II) chloride tetrahydrate ($MnCl_2 \cdot 4H_2O$) was obtained from Aldrich Chemical Co., Milwaukee, WI. Disodium (diethylenetriaminepentaacetatic acid) gadolinium (III) tetrahydrate ($Na_2[Gd(DTPA)] \cdot 4H_2O$ was prepared by the method of Wenzel et al. (20).

Venous blood was collected from a healthy, male volunteer and heparinized to prevent clotting. A stock 100 mM Gd(DTPA) blood sample was prepared by mixing 1.0 ml of whole blood with the solid $Na_2[Gd(DTPA)] \cdot 4H_2O$. Blood samples containing 100, 50, 25, 12.5, and 6.25 mM Gd(DTPA) were then prepared by successive dilution of the stock sample. A 0.5-ml aliquot of each sample was transferred to a 10-mm NMR tube for analysis. Blood samples containing 10, 5, and 2.5 mM $MnCl_2$ were prepared in an analogous manner. For measurements of relaxation times in packed red blood cells (RBC), undoped blood was centrifuged for 5–10 min and the plasma was syphoned off. 0.5-ml aliquots of the packed red blood cells were used to measure the intracellular spin–spin relaxation rate, as required for the Herbst and Goldstein (HG) analysis. The $MnCl_2$-doped blood experiments were performed 1 wk after the Gd(DTPA)-doped blood experiments and were performed with blood obtained from the same volunteer.

All NMR measurements were made with an IBM pc-10 mini-spec (IBM Instruments, Inc., Danbury, CT). The sample temperature in the NMR probe was 37°C and the Larmor frequency was 10 MHz. To obtain transverse magnetization decay curves, a Carr-Purcell-Meiboom-Gill (CPMG) sequence was applied to samples equilibrated to the probe temperature. The interpulse spacing was 240 μs and even echo maxima were sampled from a CPMG train containing 1,000 spin-echoes. The sequence was repeated 100 times with a recycle delay of 5 s. The recycle delay in these experiments was determined by data transfer limitations with the analog-to-digital device used rather than T_1 considerations. Measurement time was 15 min per sample. A maximum likelihood method, which has been previously described (21), was used to fit the decay curves to normalized biexponential functions.

Biexponential parameters of the transverse magnetization decay in perfused rat hearts were taken from those reported by Mauss et al. (19) who used a CPMG train consisting of 40 echoes spaced 16 ms apart. The details of the perfused heart preparation and NMR methods may be found in the original reference.

EXPERIMENTAL RESULTS AND ANALYSIS

The parameters obtained from biexponential fits of transverse magnetization decay curves in Gd(DTPA)- and $MnCl_2$-doped whole blood are listed in Tables 1 and 2. The quickly decaying component a, and the two apparent relaxation rates R_{2a} and R_{2b}, are listed for each concentra-

TABLE 1 Apparent volume fraction of the quickly decaying component *a*, and apparent transverse magnetization decay rates of whole blood doped with Gd(DTPA)

Gd(DTPA)	a	R_{2a}	R_{2b}
mM		*Hz*	*Hz*
63	0.300	68	28
12.5	0.530	103	41
25.0	0.602	178	64
50.0	0.682	329	94
100.0	0.741	620	281
RBC			6.1

The relaxation rate of packed RBC is also listed.

TABLE 2 **Apparent volume fraction of the quickly decaying component *a*, and apparent transverse magnetization decay rates of whole blood doped with $MnCl_2$**

$MnCl_2$	a	R_{2a}	R_{2b}
mM		*Hz*	*Hz*
2.5	0.609	176	50
5.0	0.638	340	73
10.0	0.650	690	93

tion of Gd(DTPA) or $MnCl_2$. Table 1 also contains the intracellular relaxation rate found in the packed RBC.

An HG analysis and a CL analysis were performed on the data set in Tables 1 and 2. For each concentration of Gd(DTPA) for which a biexponential fit was obtained, the HG analysis provides all the two-site exchange parameters except the intrinsic intracellular relaxation rate. This is assumed to be equal to that of packed RBC and is assumed to retain the same value at all doping levels. Each pair of concentrations in Table 1 provide the raw data for the CL analysis. With five concentrations, 10 such pairs may be constructed from the data. Among the four possible mathematical solutions, only the (+, +) solution was found to produce physically acceptable exchange parameters. In Fig. 1, the real volume fraction of the quickly decaying component g, is plotted as a function of the average Gd(DTPA) concentration of each pair used in the (+, +) CL analysis. Also plotted are the results of the HG analysis. Averaging the 10 plasma fractions obtained with the CL analysis and the five plasma fractions available from the HG analysis we obtain the following means and standard deviations:

$$g(\mathrm{CL}) = 0.77 \pm 0.05$$

$$g(\mathrm{HG}) = 0.84 \pm 0.06.$$

In both the HG and CL analysis, the plasma fraction is seen to increase at the higher concentrations of Gd(DTPA). Fig. 2 plots the intracellular–extracellular exchange rate k_{fg}, of water as a function of Gd(DTPA) concentration as calculated from both the HG and CL analyses of the data in Table 1. The HG analysis yields an exchange rate which is a monotonically increasing function of Gd(DTPA) concentration. The CL analysis yields smaller values for this exchange rate and shows no systematic dependence on Gd(DTPA) concentration below 70 mM Gd(DTPA). Excluding the rates found from doping levels above 70 mM Gd(DTPA), the mean and standard deviation of the intracellular–extracellular exchange rates are found to be

$$k_{fg}(\mathrm{CL}) = 29.5 \pm 10\ \mathrm{Hz}$$

$$k_{fg}(\mathrm{HG}) = 58.3 \pm 29\ \mathrm{Hz}.$$

The intrinsic relaxation rates at each Gd(DTPA) concentration are plotted in Fig. 3. The HG analysis provides one measurement of the plasma relaxation rate at each Gd(DTPA) concentration and assumes that the intracellular rate is 6.1 Hz at every concentration. The CL analysis of the data in Table 1 provides four separate measurements of the intrinsic relaxation rate in each compartment at every doping level. The mean of these four measurements is plotted in Fig. 3 for each concentration. The CL analysis reveals that the intracellular relaxation rate increases with Gd(DTPA) concentration, though at a much smaller rate than the extracellular component. From the data in Fig. 3, the relaxivities of

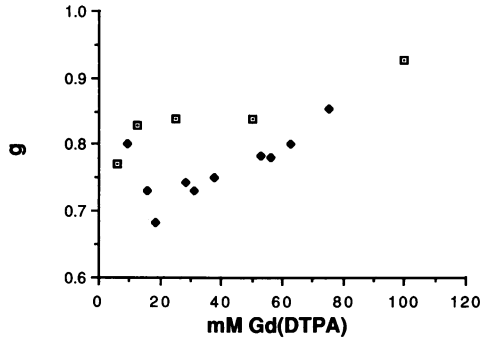

FIGURE 1 The extracellular volume fraction of exchangeable water in Gd(DTPA)-doped whole blood. The boxes represent this fraction as calculated with the HG analysis. The solid polygons represent the results of a CL analysis on the data in Table 1. In Figs. 1, 2, 4, and 6, the x coordinate for the CL data is the average of the two Gd(DTPA) or $MnCl_2$ concentrations used to extract the reported volume fraction or exchange rate.

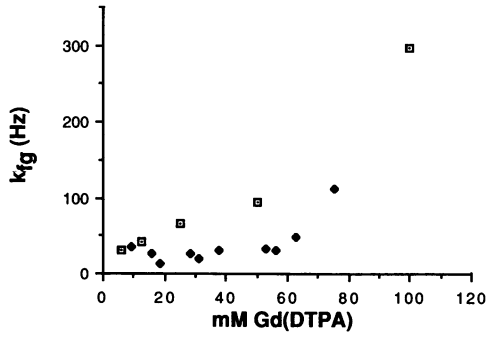

FIGURE 2 The intracellular–extracellular exchange rates as calculated from the data in Table 1. The inverse of this quantity is the average intracellular lifetime of a water molecule. The boxes are the results of an HG analysis and the solid polygons are from a CL analysis.

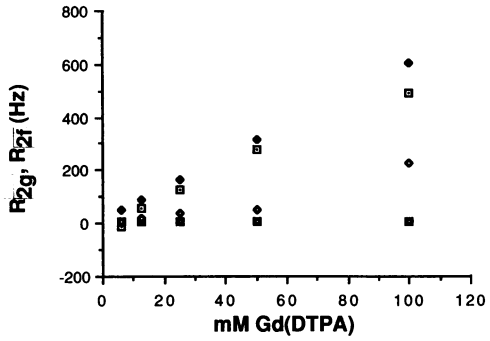

FIGURE 3 The intrinsic relaxation rates (extra- and intracellular) plotted as a function of Gd(DTPA) concentration. The boxes are from an HG analysis and polygons are from the CL analysis.

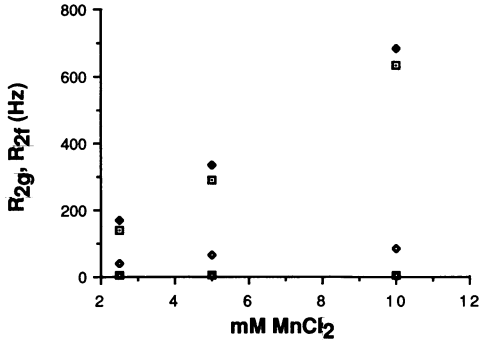

FIGURE 5 Intrinsic relaxation rates (intra- and extracellular) vs. $MnCl_2$ concentration as calculated with both HG and CL analyses.

both the intra- and extracellular fractions may be calculated from a linear fit of the relaxation rate vs. Gd(DTPA) concentration data. The plasma fraction relaxivities are found to be

$$\alpha_g(\text{CL}) = 5.9\ \text{Hz/mM[Gd(DTPA)]}$$

$$\alpha_g(\text{HG}) = 5.2\ \text{Hz/mM[Gd(DTPA)]}.$$

The relaxivities of the intracellular relaxation rates [excluding the 100 mM Gd(DTPA) point] are found to be

$$\alpha_f(\text{CL}) = 1.2\ \text{Hz/mM[Gd(DTPA)]}$$

$$\alpha_f(\text{HG}) = 0.0\ \text{(by assumption)}.$$

Figs. 4, 5, and 6 depict the results of an HG analysis and a CL analysis of the $MnCl_2$-doped blood (Table 2). Using the CL analysis, the intracellular volume fraction f is seen to remain steady at 0.33 for all three averaged concentrations while the HG analysis presents a steadily increasing intracellular volume fraction with $MnCl_2$ concentration (Fig. 4). The plot of the intrinsic relaxation rates in Fig. 5 demonstrates that a significant increase in the intracellular relaxation rate is observed when the CL analysis is applied. The most striking difference between the two methods as applied to the Mn^{2+}-doped whole blood is seen in the intracellular–extracellular exchange rates (Fig. 6). The monotonically increasing exchange rate, k_{fg}, found with the HG analysis, is seen to be independent of $MnCl_2$ concentration when the CL analysis is applied to the same data. In addition, the CL calculated exchange rate is found to be 10 Hz while the average HG calculated exchange rate is 74 Hz.

Finally, we have applied the CL analysis to the data reported by Mauss et al. for perfused rat hearts (19). Biexponential fits at seven different $MnCl_2$ concentrations were reported. Table 3 lists the results of a (+, +) CL analysis for all pairs associated with the 5 mM $MnCl_2$ perfusant solution. The first column in Table 3 lists the two $MnCl_2$ perfusant concentrations responsible for the

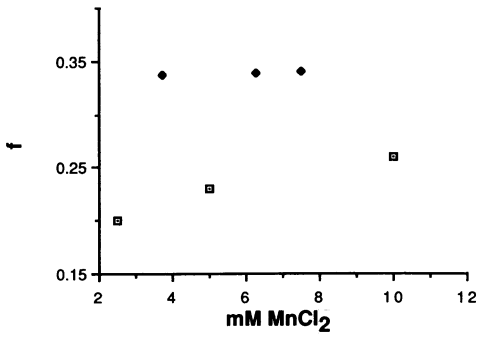

FIGURE 4 Intracellular volume fractions of exchangeable water plotted as a function of $MnCl_2$ concentration. The boxes are from the HG analysis, polygons from the CL analysis.

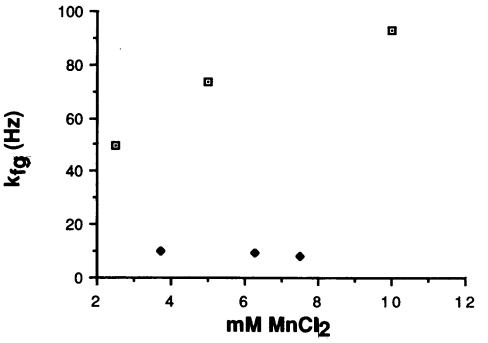

FIGURE 6 Intracellular–extracellular exchange rates vs. $MnCl_2$ concentration. The open boxes represent an HG analysis of the data and the solid polygons represent the CL analysis of the same data.

TABLE 3 **Results of a (+,+) CL analysis performed on the six pairs associated with the highest $MnCl_2$ perfusant concentration used in the perfused rat heart studies of Mauss et al (19)**

mM – mM $MnCl_2$	g	k_{gf}	R_{2g}	R_{2f}	$R_{2g'}$	$R_{2f'}$
		Hz	*Hz*	*Hz*	*Hz*	*Hz*
5–1.00	0.23	41.7	184	−16	67	−10
5–0.30	0.31	12.6	194	10	24	−8
5–0.10	0.21	53.6	181	−27	36	−32
5–0.03	0.30	15.9	193	7	15	−7
5–0.01	0.27	25.7	189	−2	20	−13
5–0.00	0.31	9.9	195	13	16	−5

six biexponential parameters used to calculate the exchange parameters appearing in that row. R_{2g} and R_{2f} are the intrinsic relaxation rates in the two compartments at the 5 mM Mn concentration and $R_{2g'}$ and $R_{2f'}$ are the intrinsic relaxation rates at the mM Mn concentration appearing as the second value in the first column. The volume fractions, exchange rates, and relaxation rates in the quickly decaying compartment were physically acceptable whereas negative values for the relaxation rates in the slowly decaying compartment were found in 9 of 12 cases.

DISCUSSION

Recently, Naritomi and co-workers (22) presented high-field in vivo spectra of both ^{23}Na and ^{1}H in gerbil brain and leg muscle. They suggested that the intra- and extracellular contribution to the spectra could be resolved with the use of a dysprosium shift reagent. They also indicated that the shifted ^{1}H spectra is one of the few methods that can noninvasively extract intra- and extracellular volume fractions, though their conclusions are not universally accepted (23, 24).

We have presented a method by which nonshift paramagnetic relaxation agents may be used to extract volume fractions, and exchange rates between volume fractions, from an analysis of biexponential transverse magnetization decay curves within the framework of the two-site exchange model. No a priori knowledge concerning the nature of the compartments or the distribution of the paramagnetic agents within the compartments is required.

Two-site exchange is undoubtedly a gross oversimplification when considered as a complete description of the state of water in structurally and chemically heterogeneous biological environments. Its conceptual simplicity, however, is not matched by mathematical simplicity when the model is applied to the interpretation of magnetic relaxation rates. As such, two-site exchange and its application to biological systems have been continuing sources of controversy. The methods presented herein can provide a relatively unambiguous test for assessing the viability of two-site exchange in various systems, whether these systems are physically separable or not.

Separable systems

Erythrocyte water exchange rates have been measured with a variety of techniques besides proton NMR (25–27). The values reported vary widely, depending on the technique employed to measure this quantity. Part of the reported variability is just a manifestation of the detailed balance relation (2) and whether or not dilution of the cells was part of the experimental protocol. However, even among similar studies, (technique, experimental protocol, etc.) wide variations of intracellular–extracellular exchange rates have been reported. For instance, a definitive temperature dependence of the exchange rate has been noted by several investigators (6, 8, 11, 14). However, while some (6, 11, 14) report an Arrhenius temperature dependence of this quantity, others (8) report a distinctly non-Arrhenius temperature dependence over similar temperature ranges. In no case was any intracellular volume dependence upon temperature (28), and its subsequent effect on the exchange rate through Eq. (2), considered. In most cases, only the intracellular lifetimes are reported, not the raw biexponential data or other relevant exchange parameters (5–9, 11–15).

The exchange rates calculated with the HG analysis of the $MnCl_2$-doped blood in our study are in good agreement with earlier reports which also used the HG analysis. Pirckle et al. (11) reported an intra–extracellular exchange rate of 61 Hz at 37°C in 1.7 mM $MnCl_2$-doped whole blood as compared to our value of 51 Hz at 2.5 mM $MnCl_2$. In addition, our HG calculated exchange rates reproduce the dependence on Mn^{2+} concentration which they reported earlier. Thus, it is not different data which we are presenting, but rather an alternate analysis and subsequent interpretation of the data.

The underlying difference between the CL and HG analyses is in the set of assumptions upon which each depends. The experimental finding is that when applied to identical data sets, significantly different values of the exchange parameters are extracted. The implication is that, for blood, the two sets of assumptions are not consistent with each other. In particular, the assumption that the intracellular relaxation rate remains uninfluenced by extracellular paramagnetic ions leads to a dependence of water exchange rates on $MnCl_2$ or Gd(DTPA) concentration. Dropping this assumption and performing a CL analysis reveals that the exchange rates and volume fractions have less of a dependence on para-

magnetic agent concentration while the intracellular relaxation rate is influenced by these agents.

The CL assumption that the volume fractions are unaffected by paramagnetic agent concentration requires some consideration when relatively large changes in the osmotic pressure of the extracellular space are induced with the addition of the agent (29, 30), though clearly isotonic experiments with differing paramagnetic concentrations may be designed. On the other hand, magnetic susceptibility differences between the intra- and extracellular spaces are enhanced with the addition of paramagnetic agents to the extracellular space. These give rise to in situ magnetic field gradients (29, 31), both intra- and extracellular for nonspherical erythrocytes, which cause additional dephasing of spins within the cell interior. Thus, the HG assumption that the intracellular relaxation rate remains unchanged with the addition of extracellular paramagnetic agents is questionable.

From the Gd(DTPA)-doped blood study, the extracellular volume fraction g, as calculated with the CL analysis, is seen to rise from values around 0.7 at the low concentrations to 0.85 at the highest concentrations (Fig. 1). This is consistent with the osmotically induced shrinking of the cells due to the high osmolarity at the greatest concentrations of Gd(DTPA) and counter-ions used (29, 30). The HG calculated plasma volume fraction is seen to be higher and to rise at lower concentrations of GD(DTPA) than the CL calculated values. The HG calculated extracellular volume fraction at the highest Gd(DTPA) concentration (0.95) is somewhat higher than might be expected from studies of erythrocyte volume changes in this osmolarity range as performed by Endre et al. (29). The intracellular volume fraction in the $MnCl_2$ studies, in which the osmolarity is not significantly changed due to the low concentrations of $MnCl_2$, is seen to be a constant 0.34 when a CL analysis is employed (Fig. 4). This fraction is significantly smaller and seen to increase from 0.16 to 0.26 with increasing $MnCl_2$ concentration when the HG analysis is applied to the same data set. Taking an average haematocrit of 0.45 and assuming the erythrocyte volume to be occupied by some 30% hemoglobin, the intracellular volume fraction is predicted to be 0.32.

An interesting difference between the Gd(DTPA) study and the $MnCl_2$ study is seen in the extracellular intrinsic relaxation rates when extrapolated to 0 mM concentration Gd(DTPA) or $MnCl_2$ (Figs. 3 and 5). The extrapolated value is much higher for the $MnCl_2$ (around 100 Hz) study than it is for the Gd(DTPA) study (around 10 Hz), regardless of the chosen analysis (CL or HG). The result is probably a consequence of the binding of Mn^{2+} ions to albumin in plasma, as first demonstrated by Mildvan and Cohn (32). This results in a dramatic decrease in the rotational correlation time of the bound Mn^{2+} ion as compared with the free ion and hence an enhancement of its contribution to the relaxation of solvent protons, especially at low concentrations, before Mn saturation of the albumin binding sites. Gd(DTPA) does not bind to either blood proteins or RBC (33) and subsequently a nonlinear dependence of the relaxation rate on Gd(DTPA) concentration is unanticipated and unobserved.

In both the $MnCl_2$- and Gd(DTPA)-doped studies, the monotonic increase of the intracellular–extracellular exchange rates with increasing paramagnetic agent concentration, as calculated with the HG analyses, is not reproduced with the CL analyses. The intracellular–extracellular exchange rates k_{fg} as calculated with the CL analysis are seen to be lower and less dependent on Gd(DTPA) concentration than those calculated with the HG analysis, though at the highest concentrations used in the Gd(DTPA) study, this rate is seen to increase regardless of the analysis. This is consistent with a smaller residence time of water within smaller cells at high osmolarities. The observed dependence of the HG calculated exchange rate on $MnCl_2$ concentration has previously been attributed to the formation of rouleau among the blood cells (6, 12, 13). Mn^{2+} ions trapped in the interstitial water pools between blood cells in rouleau have been postulated to provide a third compartment responsible for the apparent dependence of the exchange rate on $MnCl_2$ concentration. It is difficult to extend this argument to the Gd(DTPA) study since this negatively charged chelate is known to be uncomplexed with protein or blood cells and is as rotationally mobile in blood as it is in free water (33).

Rouleau formation is a well-known phenomenon in settled blood samples (34, 35) and is known to occur even before sedimentation (36) and to depend upon the presence of electrolytes, such as exogenous Mn^{2+}. It is also reasonable to assume that rouleau are responsible for a decrease in exchange rates from that associated with single cells since aggregation of blood cells increases the ratio of intracellular volume to surface area. Since the degree of aggregation is known to depend on many variables, including ionic activity (35), the different values for the exchange parameters as found in the Gd(DTPA)-doped vs. $MnCl_2$-doped blood can be accounted for. What cannot be accounted for is the difference between these values as calculated from an HG or a CL analysis performed on identical data sets. In particular the increase in the intracellular relaxation rate with increasing extracellular paramagnetic agent concentration (Figs. 3 and 5) as found with the CL analysis must be explained.

The 100–200 Å membrane separation of the paramagnetic agents from the intracellular water molecules, ignoring any Mn^{2+} uptake by red cells (37), significantly

reduces the dipole–dipole interaction between the paramagnetic agent and the intracellular water protons and completely eliminates the Fermi contact interaction as an intracellular relaxation mechanism (38, 39). However, broadening of membrane lipid resonances in the presence of nonshift paramagnetic agents in the extracellular medium indicates that the relaxation rates of some lipid protons are influenced by these agents (40, 41). Since intracellular water molecules traverse the interior of a blood cell in approximately 100–300 μs (42), frequent contact with the inner membrane lipids may contribute to the intracellular relaxation. Reducing the relaxation time of the membrane lipid protons via extracellular agents could therefore reduce the relaxation times of intracellular water protons which frequent the hydration layer of the inner membrane in some fast exchange limit.

The most important cross-membrane relaxation mechanism, however, most probably arises from the large differences in magnetic susceptibility between intra-and extracellular spaces that are induced by paramagnetic agents confined to the extracellular space (29, 31, 43). These give rise to microscopic magnetic field gradients at the cell surfaces which have previously been exploited to monitor transport of small molecules such as alanine and lactate across erythrocyte membranes (29). Diffusion of intracellular spins in and out of these gradients results in an additional spin-dephasing mechanism and subsequent increase in the spin–spin relaxation rate within the red cell. Extracellular paramagnetic agents, therefore, can and most probably do, influence intracellular relaxation rates. In fact, it is somewhat easier to justify an intracellular relaxivity than it is to justify a dependence of water transport processes on paramagnetic agent concentrations. The ability of the CL analysis to measure the increase in relaxation rate within the cell may prove of great utility in studying the influence of cell shape upon induced microscopic field gradients (29).

Inseparable systems

We applied the CL method of analysis to the perfused rat heart data in an attempt to determine whether intra- and extracellular water compartmentalization is an important feature of the observed biexponential relaxation. Mauss et al. (19) suggested that the linear dependence of the larger of the two apparent relaxation rates on $MnCl_2$ concentration in the perfusant indicated that the protons responsible for this signal arose from the extracellular water protons where the agent was distributed. The apparent size of this component ranged from 0.22 to 0.65 at the different $MnCl_2$ concentrations used in their study. The (+, +) CL analysis of the pairs associated with the 5 mM Mn^{2+} concentration yields a real volume fraction of the quickly decaying component (g, Table 3) of 0.27 ± 0.04. The exchange rate k_{gf} is found to be 27 ± 18 Hz. We remark that Sobol and co-workers reported a value of 29 ± 9 Hz for the chemical exchange between bulk and bound water in excised mouse muscle (16). Assuming that g and k_{gf} reflect the actual extracellular volume fraction and extracellular–intracellular exchange rate, we calculate [through Eq. (2)] an intracellular water residence time of 100 ms. For comparison, Tanner (44) has estimated intracellular residence times of 430 ms in in vitro frog muscle using a different NMR technique. However, the "reasonable" values found for the "extracellular" fraction of exchanging protons and intracellular water residence time come from an analysis which also produces physically unacceptable values for the "intracellular" relaxation rate and so must be viewed with a measure of caution.

The negative relaxation rates for the f fraction in Table 3 may partially reflect the difficulty of imposing such an exacting analysis upon a system which only grossly approximates a two-site exchange system. Biological compartmentalization of water includes mitochondrial reservoirs and other intracellular organelles. In addition, a distribution of cell volumes rather than an idealized intracellular volume would more accurately reflect the physical situation. However, an equally likely explanation is the error associated with the experimental biexponential input parameters. Such errors are known to propagate strongly in nonlinear two-site exchange analyses, as discussed in detail by Pirckle et al. (11). The CPMG train used by Mauss et al. (19) sampled only 40 echo maxima every 16 ms, yet they report short component T_2 values as low as 5 ms. Undersampling of the decay curve can lead to significant errors in biexponential parameters and subsequently in the calculated exchange values.

Finally, we use the (+, +) CL analysis on a set of data which Fung and Puon (10) used to discredit the notion that biexponential decay in mouse muscle arose from intra- and extracellular water compartments. We note that several arguments were presented, including the effects of deuteration, and glycerination on the T_2 decay curves, as well as postmortem changes in the decay, to cast doubt upon an intracellular–extracellular water exchange phenomenon as the source of biexponential decay in mouse muscle. However, a direct argument involving a two-site exchange analysis of transverse decay data collected at two different field strengths was also presented and it is this argument which we reconsider in the light of the CL analysis.

Measurements of the transverse magnetization decay were performed at two different magnetic field strengths and the results decomposed into biexponential functions. The data of Fung and Puon is presented in Table 4. If we assume that changing the field strengths alters only the intrinsic relaxation rates and not the volume fractions and

TABLE 4 **Data taken from Fung and Puon's biexponential fits to transverse decay curves in mouse muscle at two different field strengths**

Larmor frequency	a	R_{2a}	R_{2b}
MHz		*Hz*	*Hz*
9.2	0.95	18.52	3.7
16.0	0.95	20.83	2.7

exchange rates between these fractions, the assumptions behind the CL analysis apply (as long as a substantial chemical shift is not induced). Changing the field strength replaces the introduction of a contrast agent to the medium. A (+, +) CL analysis of the data in Table 4 results in a perfectly acceptable set of two-site exchange parameters. Namely, calculated volume fractions f and g of 0.95 and 0.05, extremely small, but positive, exchange rates, and intrinsic relaxation rates practically identical to the apparent relaxation rates listed in Table 4.

Fung and Puon (10) used Tanner's (44) value of 430 ms for τ_a, the intracellular residence time of a water molecule in frog muscle, and used their own measured value of the apparent volume fraction of the quickly decaying component a, as the actual volume fraction of intracellular water. Upon reinserting these values and the apparent relaxation rates back into the two-site exchange equations [Appendix Eqs. (A1) to (A4)], the intrinsic relaxation rates turned out to be "either imaginary or negative, clearly an unacceptable result."

The basis for this particular defrocking of the two-site exchange model in muscle is in error. An independent measurement of τ_a, or in our notation $1/k_{fg}$, is an acceptable starting point for a two-site exchange analysis. Once this measurement is accepted, however, a single biexponential fit is all that is required to extract the remaining two-site exchange parameters (cf. Eq. (13)]. Instead, Fung and Puon (10) overspecified the number of known variables by assuming that the quickly decaying volume fraction was indeed, the real, intracellular volume fraction. To do so is equivalent to assuming negligible exchange, a result paradoxically in agreement with the CL analysis of their data.

CONCLUSION

The method we have presented links apparent relaxation rates and volume fractions, as obtained from biexponential fits of the transverse magnetization decay at two doping levels, directly with the two-site exchange parameters. The method has been applied to both separable and inseparable systems. In the former case, comparison with results previously reported was possible. In whole blood, significant differences between the exchange parameters as calculated with the CL method and with the HG method were found, though both yield physically acceptable values and the results of the HG analysis are consistent with other HG analyses reported in the literature. We conclude that replacing the assumption that intracellular relaxation rates are uninfluenced by extracellular paramagnetic agents, with the assumption that paramagnetic agents do not influence water exchange rates or volume fractions, leads to a substantially different interpretation of identical data sets. In this sense, the CL analysis may provide more reliable measures of exchange parameters than an HG analysis as well as providing additional information pertaining to cross-membrane relaxation processes and in situ microscopic field gradients.

We have demonstrated the application to inseparable systems by applying the analysis to perfused rat heart data, as reported by Mauss et al. (19). Physically acceptable volume fractions, exchange rates, and the larger of the two intrinsic relaxation rates were extracted from a limited portion of the reported data. The volume fractions so calculated may reflect intra- and extracellular water compartmentalization, as suggested by Mauss et al., though this is not the only interpretation possible. The complexity of the system and/or the inherent errors in biexponential input parameters may be responsible for the failure of the model to yield a complete set of physically acceptable exchange parameters in perfused heart as opposed to blood. The present analysis cannot be used to differentiate between these two explanations. Higher $MnCl_2$ perfusant concentrations, which make the decay curve particularly sensitive to exchange processes, and greater sampling of the decay curve would be helpful in further assessing the applicability of two-site exchange in perfused heart.

Some potential practical applications of the method may be considered. Besides erythrocyte exchange parameters, water transport properties in liposomes (45) may be studied with the present technique. Knowledge of water transport rates across liposome membranes can help in predicting the relaxivities of liposome-entrapped paramagnetic agents, and hence be of use in predicting their value as magnetic resonance imaging (MRI) contrast agents in vivo. The applicability of two-site exchange in tissue simulating gels may be tested by preparing paramagnetically doped gels and applying the CL analysis to these physically inseparable systems. Two-site exchange has often been used as a description of the state of water in gels (46, 47), though Outhred and George (48) have suggested that such a model is too simple.

In MRI, the clinical use of paramagnetic contrast agents for image enhancement is growing (49, 50) and the multiexponential behavior of transverse magnetiza-

tion decay in tissue is firmly established (10, 16, 17, 51, 52). The potential of multiexponential image analyses to improve diagnostic specificity with MRI is now also confirmed (53, 54). The mathematical transformation presented above, in combination with biexponential analysis of MR images and the introduction of contrast agents, may provide a framework for testing models of exchange processes directly from postprocessing of MR images.

APPENDIX

The starting point of the analysis is the set of relations between the apparent quantities in a biexponential fit and the real parameters of the two-site exchange model. Let the normalized biexponential be

$$M(t)/M_0 = a \exp(-R_{2a}t) + b(-R_{2b}t). \quad \text{(A0)}$$

The two-site exchange equations linking the real parameters to the apparent parameters in Eq. (A0) are (1–3, 11, 13):

$$R_{2a} = C_1 - C_2 \quad \text{(A1)}$$

$$R_{2b} = C_1 + C_2 \quad \text{(A2)}$$

where

$$C_1 = (R_{2g} + R_{2f} + k_{gf} + k_{fg})/2 \quad \text{(A3)}$$

$$C_2 = [(R_{2f} - R_{2g} + k_{fg} - k_{gf})^2 + 4k_{gf}k_{fg}]^{1/2}/2 \quad \text{(A4)}$$

and

$$b = \tfrac{1}{2} - [(f - g)(R_{2g} - R_{2f}) + k_{gf} + k_{fg}]/(4C_2) \quad \text{(A5)}$$

$$a = 1 - b. \quad \text{(A6)}$$

Since C_1 and C_2 are real, positive quantities, this identifies R_{2b} as the largest of the two relaxation rates in Eq. (3). The apparent volume fraction of the quickly decaying component is then identified as b in this case. Our goal is to derive the relationship expressed by Eqs. (13) and (14) from these expressions. We begin by making a useful definition:

$$\alpha = 2C_2(1 - 2b). \quad \text{(A7)}$$

From Eq. (A5), solve for the difference in intrinsic relaxation rates to obtain

$$R_{2f} - R_{2g} = (k_{gf} + k_{fg} - \alpha)/(f - g). \quad \text{(A8)}$$

Substitute this into Eq. (A4), multiply by 2, and square both sides to obtain

$$4C_2^2 = [(k_{gf} + k_{fg} - \alpha)/(f - g) + k_{fg} - k_{gf}]^2 + 4k_{gf}k_{fg}. \quad \text{(A9)}$$

We now use the volume normalization and detailed balance relations, (1) and (2), to eliminate f and k_{fg} from Eq. (A9) and rearrange the resulting expression to obtain a quadratic in k_{gf}.

$$4gk_{gf}^2 - 8\alpha g(1 - g)k_{gf} + (1 - g)[\alpha^2 - 4C_2^2(1 - 2g)^2] = 0. \quad \text{(A10)}$$

Applying the quadratic formula to find the roots of Eq. (A10) and simplifying the resulting expression leads to the following relation for k_{gf} in terms of α, g, and C_2:

$$k_{gf} = \alpha(1 - g) \pm \{[g(1 - g)(1 - 2g)^2(4C_2^2 - \alpha^2)]^{1/2}\}/2g. \quad \text{(A11)}$$

This is equivalent to expressions (13) and (14). To obtain the (+, +) solution for g we choose + signs in Eqs. (13) and (14), multiply both by $2g$ and subtract the two relations to obtain:

$$\delta 2g(1 - g) = -[g(1 - g)(1 - 2g)^2]^{1/2}\Gamma_-, \quad \text{(A12)}$$

where we have used the definitions (11) and (12). Squaring both sides, expanding and collecting powers of g leads to a quadratic in g whose roots are given by Eq. (15).

The antisymmetric solutions utilize Γ_+ in (12). The (+, −) solution is:

$$g = [1 \pm \delta/(\Gamma_+^2 + \delta^2)^{1/2}]/2 \quad \text{(A13)}$$

and

$$k_{gf} = \alpha(1 - g) + [g(1 - g)(2g - 1)^2(4C^2 - \alpha^2)]^{1/2}/(2g) \quad \text{(A14)}$$

or

$$k_{gf} = \beta(1 - g) - [g(1 - g)(2g - 1)^2(4F^2 - \beta^2)]^{1/2}/(2g). \quad \text{(A15)}$$

When applied to the 12.5 and 6.25 mM Gd(DTPA) data in Table 1, we obtain

g	k_{gf}	R_{2g}	R_{2f}	$R_{2g'}$	$R_{2f'}$
0.4	5.18	36.1	99.3	62.4	24.9

All the exchange parameters are physically reasonable but, at the 12.5 mM concentration, the f fraction has the largest relaxation rate ($R_{2f} > R_{2g}$) and at the 6.25 mM concentration, the g fraction has the largest relaxation rate ($R_{2g'} > R_{2f'}$). It is physically unreasonable for the intracellular volume fraction to have the smallest relaxation rate at one concentration and the largest at another, for concentrations in this range. This feature suggests that the antisymmetric solutions are physically unacceptable even if all the exchange parameters are real and positive.

TABLE A1 Conversion table indicating the notation used in this work compared with that used by Herbst and Goldstein

This work	Herbst and Goldstein
a	$P_{a'}$
b	$P_{b'}$
R_{2a}	$1/T_{2a'}$
R_{2b}	$1/T_{2b'}$
f	P_b
g	P_a
k_{gf}	$1/\tau_a$
k_{fg}	$1/\tau_b$
R_{2g}	$1/T_{2a}$
R_{2f}	$1/T_{2b}$

The relations given by Herbst and Goldstein yield the real volume fractions and exchange rates in terms of the three experimental parameters obtained from a biexponential fit to the decay curves. They may be found in the Appendix of Herbst and Goldstein (13). Below is Table A1 which converts the notation used in this work with the notation of Herbst and Goldstein. Our notation uses less primed variables and division signs. Eq. (A9) of Herbst and Goldstein (13) is a definition of C_2 and not of C_1.

We thank Dr. Carmen Solorzano for providing the Gd(DTPA) compound used in the doped blood studies. Her assistance in the preparation and NMR measurements of the blood samples is greatly appreciated. We also thank Dr. Martin Kushmerick for helpful discussions during the course of this work.

This study was supported in part by National Institutes of Health grants 5 T32 CA09536-04, 5 R01 NS23093-03, and 2 P01 CA41167-02AICC; and National Institute of Aging grant 2 P01 AG04953-04. Dr. Jolesz is the recipient of National Institutes of Health grant 5 K04 NS01083-03.

Received for publication 6 June 1988 and in final form 7 September 1988.

REFERENCES

1. McConnel, H. M. 1958. Reaction rates by nuclear magnetic resonance. *J. Chem. Phys.* 28:430–431.
2. Woessner, D. E. 1960. Nuclear transfer effects in nuclear magnetic resonance pulse experiments. *J. Chem. Phys.* 35:41–48.
3. Zimmerman, J. R., and W. E. Brittin. 1957. Nuclear magnetic resonance studies in multiple phase systems: lifetime of a water molecule in an adsorbing phase on silica gel. *J. Phys. Chem.* 61:1328–1333.
4. Carver, J. P., and R. E. Richards. 1972. A general two-site solution for chemical exchange produced dependence of T_2 upon the Carr-Purcell pulse separation. *J. Magn. Reson.* 6:89–105.
5. Conlon, T., and R. Outhred. 1972. Water diffusion permeability of erythrocytes using a nuclear magnetic resonance technique. *Biochim. Biophys. Acta.* 288:354–361.
6. Conlon, T., and R. Outhred. 1978. The temperature dependence of erythrocyte water diffusion permeability. *Biochim. Biophys. Acta.* 511:408–418.
7. Morariru, V. V., and G. Benga. 1977. Evaluation of a nuclear magnetic resonance technique for the study of water exchange through erythrocyte membranes in normal and pathological subjects. *Biochim. Biophys. Acta.* 469:301–310.
8. Morariru, V. V., V. I. Pop, O. Popescu, and G. Benga. 1981. Effects of temperature and pH on the water exchange through erythrocyte membranes: nuclear magnetic resonance studies. *J. Membr. Biol.* 62:1–5.
9. Fabry, M. E., and M. Eisenstadt. 1978. Water exchange across red cell membranes. II. Measurement by nuclear magnetic resonance T_1, T_2, and T_{12} hybrid relaxation: the effects of osmolarity, cell volume and medium. *J. Membr. Biol.* 42:375–398.
10. Fung, B. M., and P. S. Puon. 1981. NMR transverse relaxation in muscle water. *Biophys. J.* 33:27–37.
11. Pirckle, J. L., D. L. Ashley, and J. H. Goldstein. 1979. Pulse nuclear magnetic resonance measurements of water exchange across the erythrocyte membrane employing a low Mn concentration. *Biophys. J.* 25:389–406.
12. Herbst, M. D., and J. H. Goldstein. 1984. Monitoring red blood cell aggregation with nuclear magnetic resonance. *Biochim. Biophys. Acta.* 805:123–126.
13. Herbst, M. D., and J. H. Goldstein. 1984. Cell water transport measurement by NMR: a three compartment model which includes cell aggregation. *J. Magn. Reson.* 60:299–306.
14. Caines, G. H., C. F. Morgan, R. C. Long, Jr., and J. H. Goldstein. 1987. Transverse relaxation of saline and plasma using Mn(II), HSA-EDTA-Mn, and HSA-EDTA-Gd: application to erythrocyte water exchange. *Magn. Reson. Med.* 5:269–277.
15. Getz, D., J. F. Gibson, R. N. Sheppard, K. J. Micklem, and C. A. Pasternak. 1979. Manganese as a calcium probe: electron paramagnetic resonance and nuclear magnetic resonance spectroscopy of intact cells. *J. Membr. Biol.* 50:311–329.
16. Sobol, W. T., L. G. Cameron, W. R. Inch, and M. M. Pintar. 1986. Modeling of proton spin relaxation in muscle tissue using nuclear magnetic resonance spin grouping and exchange analysis. *Biophys. J.* 50:181–191.
17. Sobol, W. T., and M. M. Pintar. 1987. NMR spectroscopy of heterogeneous solid-liquid mixtures: spin grouping and exchange analysis of proton spin relaxation in tissue. *Magn. Reson. Med.* 4:537–554.
18. Edzes, H. T., and E. T. Samulski. 1978. The measurement of cross-relaxation effects in the proton NMR spin-lattice relaxation of water in biological systems: hydrated collagen and muscle. *J. Magn. Reson.* 31:207–217.
19. Mauss, Y., D. Grucker, D. Fornasiero, and J. Chambron. 1985. NMR compartmentalization in the perfused rat heart. *Magn. Reson. Med.* 2:187–194.
20. Wenzel, T. J., M. E. Ashley, and R. E. Sievers. 1982. Water-soluble paramagnetic relaxation reagents for carbon-13 nuclear magnetic resonance spectrometry. *Anal. Chem.* 54:615–621.
21. Sandor, T., A. R. Bleier, P. W. Ruenzel, D. F. Adams, and F. A. Jolesz. 1988. Application of the maximum likelihood principle to separate exponential terms in T_2 relaxation of nuclear magnetic resonance. *Magn. Reson. Imaging.* 6:27–40.
22. Naritomi, H., M. Kanashiro, M. Sasaki, Y. Kuribayashi, and T. Sawada. 1987. In vivo measurements of intra- and extracellular Na^+ and water in the brain and muscle by nuclear magnetic resonance spectroscopy with shift reagent. *Biophys. J.* 52:611–616.
23. Burstein, D. 1988. On the in vivo detection of intracellular water and sodium by nuclear magnetic resonance with shift reagents. *Biophys. J.* 54:191–192.
24. Naritomi, H., M. Sasaki, Y. Kuribayashi, T. Sawada, and M. Kanashiro. 1988. Validity of in vivo nuclear magnetic resonance methods in measurement of intracellular water and sodium. *Biophys. J.* 54:193.
25. Paganelli, C. V., and A. K. Solomon. 1957. The rate of exchange of tritiated water across the human red cell membrane. *J. Gen. Physiol.* 41:259–277.
26. Shporer, M., and M. M. Civan. 1975. NMR study of ^{17}O from $H_2{}^{17}O$ in human erythrocytes. *Biochim. Biophys. Acta.* 385:81–87.
27. Andrasko, J. 1976. Water diffusion permeability of human erythrocytes studied by a pulsed gradient NMR technique. *Biochim. Biophys. Acta.* 428:304–311.

28. Farmer, R. E. L., and R. I. Macey. 1970. Perturbation of red cell volume: rectification of osmotic flow. *Biochim. Biophys. Acta.* 196:53–65.

29. Endre, Z. H., P. W. Kuchel, and B. E. Chapman. 1984. Cell volume dependence of ^{1}H spin-echo NMR signals in human erythrocyte suspensions: the influence of in situ field gradients. *Biochim. Biophys. Acta.* 803:137–144.

30. Ponder, E. 1948. Hemolysis and Related Phenomena. Grune & Stratton, Inc., New York. 50–114.

31. Brindle, K. M., F. F. Brown, I. D. Campbell, C. Grathwohl, and P. W. Kuchel. 1979. Application of spin-echo nuclear magnetic resonance to whole cell systems. *Biochem. J.* 180:37–44.

32. Mildvan, A. S., and M. Cohn. 1963. Magnetic resonance studies of the interaction of the manganous ion with bovine serum albumin. *Biochemistry.* 2:910–919.

33. Koenig, S. H., M. Spiller, R. D. Brown III, and G. Wolf. 1986. Relaxation of water protons in the intra- and extracellular regions of blood containing Gd(DTPA). *Magn. Reson. Med.* 3:791–795.

34. Jan, K.-M. 1979. Red cell interactions in macromolecular suspension. *Biorheology.* 16:137–148.

35. Jan, K.-M., and S. Chien. 1973. Influence of ionic composition of fluid medium on red cell aggregation. *J. Gen. Physiol.* 61:655–668.

36. Fabry, T. L. 1987. Mechanism of erythrocyte aggregation and sedimentation. *Blood.* 70:1572–1576.

37. Weed, R. I., and A. Rothstein. 1961. The uptake of divalent manganese ion by mature normal human blood cells. *J. Gen. Physiol.* 44:301–314.

38. Bloembergen, N., and L. O. Morgan. 1960. Proton relaxation times in paramagnetic solutions: effects of electron spin relaxation. *J. Chem. Phys.* 34:842–850.

39. Abragam, A. 1962. Principles of Nuclear Magnetism. Clarendon Press, Oxford, England. 159–215.

40. Bergelson, L. D. 1978. Paramagnetic hydrophilic probes in NMR investigations of membrane systems. *Methods Membr. Biol.* 9:275–335.

41. Bennet, H. F., H. M. Swartz, R. D. Brown III, and S. H. Koenig. 1987. Modification of lipid protons by molecular oxygen and nitroxides. *Invest. Radiol.* 22:502–507.

42. Gillis, P., and S. H. Koenig. 1987. Transverse relaxation of solvent protons induced by magnetized spheres: application to ferritin, erythrocytes, and magnetite. *Magn. Reson. Med.* 5:323–345.

43. Villringer, A., B. R. Rosen, J. W. Belliveau, J. L. Ackerman, R. B. Lauffer, R. B. Buxton, Y. S. Chao, V. J. Wedeen, and T. J. Brady. 1988. Dynamic imaging with lanthanide chelates in normal brain: contrast due to magnetic susceptibility effects. *Magn. Reson. Med.* 6:164–174.

44. Tanner, J. E. 1979. Self-diffusion of water in frog muscle. *Biophys. J.* 28:107–116.

45. Andrasko, J., and S. Forsen. 1974. NMR study of rapid water diffusion across lipid bilayers in dipalmitoyl lecithin vesicles. *Biochem. Biophys. Res. Commun.* 60:813–819.

46. Kaneoke, Y., F. Masahiro, S. Inao, K. Saso, K. Yoshida, Y. Motegi, M. Motomu, and A. Izawa. 1987. Spin-lattice relaxation times of bound-water—its determination and implications for tissue discrimination. *Magn. Reson. Imaging.* 5:415–420.

47. Fullerton, G. D., I. L. Cameron, and V. A. Ord. 1984. Frequency dependence of magnetic resonance spin-lattice relaxation of protons in biological materials. *Radiology.* 151:135–138.

48. Outhred, R. K., and E. P. George. 1973. A nuclear magnetic resonance study of hydrated systems using the frequency dependence of the relaxation processes. *Biophys. J.* 13:83–96.

49. Carr, D. H., J. Brown, G. M. Bydder, R. E. Steiner, H.-J. Weinmann, U. Speck, A. S. Hall, and I. R. Young. 1984. Gadolinium-DTPA as a contrast agent in MRI: initial experience in 20 patients. *AJR (Am. J. Roentgenol.).* 143:215–224.

50. Runge, V. M., J. A. Clanton, C. M. Lukehart, C. L. Partain, and A. E. James, Jr. 1983. Paramagnetic agents for contrast-enhanced NMR imaging: a review. *AJR (Am. J. Roentgenol.).* 141:1209–1215.

51. Peemoeller, H., and M. M. Pintar. 1979. NMR multiwindow analysis of proton local fields and magnetization distribution in natural and deuterated mouse muscle. *Biophys. J.* 28:339–356.

52. Barthwal, R., M. Hohn-Berlage, and K. Gersonde. 1986. In vivo proton T_1 and T_2 studies on rat liver: analysis of multiexponential relaxation processes. *Magn. Reson. Med.* 3:863–875.

53. Dumitresco, B. E., J. P. Armspach, D. Gounot, D. Grucker, Y. Mauss, J. Steibel, D. Wecker, and J. Chambron. 1986. Multiexponential analysis of T_2 images. *Magn. Reson. Imaging.* 4:445–448.

54. Staemmler, M., and K. Gersonde. 1986. Echo shape analysis and image size adjustment on the level of echoes: improvement of parameter-selective proton images. *Magn. Reson. Med.* 3:418–424.